ELSEVIER

Biophysical Chemistry 101–102 (2002) 593–609

Biophysical Chemistry

www.elsevier.com/locate/bpc

Use of T4 lysozyme charge mutants to examine electrophoretic models

Jennifer A. Durant[a], Chuanying Chen[b], Thomas M. Laue[a], Thomas P. Moody[a], Stuart A. Allison[b,*]

[a]*Center to Advance Molecular Interaction Science, Department of Biochemistry and Molecular Biology, Rudman Hall, University of New Hampshire, Durham, NH 03824-3544, USA*
[b]*Department of Chemistry, Georgia State University, University Plaza, Atlanta, GA 30303, USA*

Received 11 December 2001; received in revised form 23 January 2002; accepted 23 January 2002

Abstract

The electrophoretic mobility of a macro-ion is affected in a complex manner by a variety of forces that arise from the applied field. Coupling of the macro-ion and small-ion flows gives rise to non-conserved forces that are greater than those expected from ordinary hydrodynamic considerations. It is difficult to separate the steady-state hydrodynamic and electrodynamic contributions to the macro-ion mobility. Membrane-confined electrophoresis (MCE), a free solution technique, provides an experimental means by which to gain insight into these contributions. In this work we used MCE steady-state electrophoresis (SSE) of a series of T4 lysozyme charge mutants to investigate these effects and to examine the existing theoretical descriptions. These experiments isolate the effects of charge on electrophoretic mobility and permit a unique test of theories by Debye–Hückel–Henry, Booth and Allison. Our results show that for wild type (WT) T4, where divergence is expected to be greatest, the predicted results are within 15, 8 and 1%, respectively, of experimental SSE results. Parallel experiments using another free-solution technique, capillary electrophoresis, were in good agreement with MCE results. The theoretical predictions were within 20, 13 and 5% of CE mobilities for WT. Boundary element modeling by Allison and co-workers, using continuum hydrodynamics based on detailed structural information, provides predictions in excellent agreement with experimental results at ionic strengths of 0.11 M.

Keywords: Protein charge; Electrostatic; Boundary element modeling; Free-solution electrophoresis; T4 lysozyme; Charge mutants

*Corresponding author. Fax: +1-404-651-1986.
E-mail address: chesaa@panther.gsu.edu (S.A. Allison).

0301-4622/02/$ - see front matter
PII: S0301-4622(02)00168-0

1. Introduction

With the introduction of capillary electrophoresis, there has been renewed interest in 'free solution', or 'free boundary' electrophoresis [1–5]. This interest stems, in part, from the fact that free boundary electrophoresis is an intrinsically absolute method that provides physical first-principle measurements. The ability to rigorously interpret electrophoretic data would provide biologists with methods for quantitatively assessing the charge on macro-ions. This ability, in turn, would allow for the correlation of charge with other macro-ion characteristics, such as solubility, stability and binding strength. Until recently, electrophoretic data have remained intractable to rigorous interpretation, with few exceptions. The exceptions are special limiting cases in which the macro-ion is assumed to be infinitely dilute, and describable by a relatively simple structural model. These structural models include spheres with a symmetric charge distribution [6–9]; long, uniformly charged cylinders [10,11]; or 'thin double-layer' models [12–15]. The work described here is directed at extending the interpretability of electrophoretic data to a wider range of macro-ions and solvent conditions. The recent development of an iterative boundary element (BE) methodology has made it possible to model dilute, rigid, model polyions of arbitrary shape and charge distribution [16]. Over the last few years, it has been applied to a number of biochemical systems [17–20].

Unlike previous studies, however, in the present work we focus our attention on the influence of total charge and charge distribution on absolute mobility, holding other factors, such as macro-ion conformation, salt type and concentration, etc., constant.

In earlier work, the charge on the macro-ion either was not varied or was varied by changing the solution pH [17]. Because of this, it is hard to interpret the electrophoretic effects *purely* in terms of the charge on the macro-ion. Thus, we have taken a different approach in this work and changed charge not by changing solvent conditions, but by using a series of charge mutants.

In order to test the relationship between the charge on a macro-ion and various models describing electrophoretic mobility, it is necessary to have a clear concept of what constitutes macro-ion charge. Ordinarily, when calculating valence of macro-ions, protons are the only ions considered. At neutral pH for proteins, the valence is a signed, integral value calculated as the signed sum of the valences of the functional groups, while for nucleic acids it is usually assumed to equal the number of phosphates. At any instant, however, individuals in a group of macro-ions may have different valences due to the binding of small ions, giving rise to several distinct charged species. For clarity, we define z, the *average* valence or formal charge, as the charge on the macro-ion within its hydrodynamic shear surface [21] under the solvent conditions and Q as the product of z and e, the elementary charge. The effective charge, z_{eff}, is the valence reduced by flow effects (i.e. electrophoretic effect and ion relaxation), and thus $Q_{\mathrm{eff}} = z_{\mathrm{eff}}e$. Both z and z_{eff} are time-averaged values. Often the individual pK_{a} values of a protein are either not known, or the conditions under which they were measured are different from those used in electrophoretic experiments, making accurate calculation of the formal charge difficult. By mutating amino acids with side-chain pK_{a} values distant from the pH at which measurements are made, the *change* in the formal charge of the mutants from the wild type protein may be known with greater accuracy than the absolute formal charge values. Thus, it is advantageous to explore the correlation between charge and mobility through charge mutants.

In general, the electrophoretic characteristics of dilute macro-ion solutions depend not only on the properties of the macro-ion itself, but also on the properties of the counterions and, to a lesser extent, of the co-ions. Overbeek [6] derived the first general formulation of the coupled steady-state hydrodynamic, ion transport and electrodynamic differential equations, which he then applied to the electrophoretic transport of a sphere of low charge in a weak external field. More general treatments of a macro-ion modeled as a charged sphere followed [7–9].

Coupling of the macro-ion and small-ion flows gives rise to non-conserved forces that are greater than those expected from ordinary hydrodynamic considerations [8]. Since the ion atmosphere and

the macro-ion tend to move in opposite directions when an electric field is present, there is a non-conservative, steady-state force on the macro-ion that is due to the resulting counter-flow of fluid. This is commonly referred to as the 'electrophoretic effect' [8,22]. The electrophoretic effect does not include the force generated by the distortion of the ion atmosphere from its equilibrium distribution. The tendency of the ion atmosphere and macro-ion to move in opposite directions, however, does distort the ion atmosphere from its equilibrium distribution, and this in turn gives rise to an additional force, referred to as the 'ion relaxation effect' [8]. Both the electrophoretic effect and the ion relaxation effect decrease the velocity of the macro-ion from that which would be predicted from simple hydrodynamic and electrostatic considerations. The electrophoretic effect significantly reduces the mobility of any macro-ion, whereas the ion relaxation effect is only significant for more highly charged macro-ions [8,23].

The magnitude of the electrophoretic and ion relaxation effects is dependent in a complex manner on the properties of the solvent and the macro-ion. Furthermore, both effects vary linearly with the electric field, making it impossible to determine their contributions by varying the field strength over an experimentally reasonable range [6–8,18]. The contribution of formal charge to the electrophoretic mobility of a macro-ion is also expected to vary linearly with the electric field. Thus, as conducted at present, electrophoretic mobility experiments by themselves do not provide sufficient information for characterization of the formal charge of a macro-ion.

However, in the last few years, Allison and coworkers [16–18] have used the transport theory of Overbeek [6] and Booth [7], as well as O'Brien and White [9], to develop a boundary element method that models the electrophoresis of infinitely dilute, rigid macro-ions of arbitrary size, shape and charge distribution. The modeling incorporates structural and titration data, and applies the transport theory to predict the electrophoretic mobility of macro-ions. This method has produced results that are in good agreement with the experimentally determined mobilities of hen egg-white lysozyme [17], short duplex DNA fragments [18,19] and duplex DNA fragments of variable length [20].

These last few years have also seen the development of a membrane-confined analytical electrophoresis (MCE) instrument [24]. This instrument is capable of providing accurate measurements of the effective charge [25]. This effective charge is used, along with the translational diffusion coefficient, to calculate mobility. In this paper, experimental measurements of the electrophoretic properties of T4 bacteriophage lysozyme and charge mutants have been compared with the corresponding boundary-element modeling predictions. The results reveal that SSE, CE and BE results are in excellent agreement at 0.11 M ionic strength. MCE, which requires much less material than titration and NMR studies, can therefore be used to obtain the formal charge of a globular protein.

2. Materials and methods

2.1. Proteins

Clones of wild type T4 lysozyme and charge mutants (courtesy B. Matthews, University of Oregon) were expressed and purified based on methods described elsewhere [26]. The mutations were as follows: SM (R119E), DM (K16E/R154E), TM (R119E/K135E/K147E) and QM (K16E/R119E/K135E/K147E). Purity with respect to size and charge was addressed by SDS-PAGE and CE and showed that samples were $>$ 99% homogeneous.

2.2. Solvent

All solvents were prepared using reagent grade chemicals and distilled, deionized water. Buffer pH was determined using an Orion 520A pH meter. Specific conductance was measured with a VWR 1054 conductivity meter and a platinum (>5 mS cm^{-1}) or gold (<5 mS cm^{-1}) probe. Samples were analyzed in 10 mM bis-Tris–propane (BTP), 100 mM KCl, pH 7.5, unless otherwise noted.

2.3. pK_a values

In order to calculate the formal charge, it is necessary to have estimates of the pK_a values of the titratable groups. Determination of protein

residue pK_a values is complicated by their dependence on ionic strength, macro-ion charge and the potential for ion pair formation [27]. Consequently, there is uncertainty in the formal charge. In this work we have attempted to estimate the uncertainty by calculating the formal charge using various estimates of the pK_a values. The formal charge is reported as an average of three calculations at pH 7.5 and the error estimated for the 90% confidence level. The pK_a values used are given in Table 1. The first set of values was taken from E. Anderson's 1992 thesis dissertation [28]. The second and third sets make use of general textbook values [29,30] combined with the NMR values for His31 and Asp70, which form a salt bridge [28,31].

2.4. Capillary electrophoresis

Capillary zone electrophoresis was carried out at 20 °C with an eCap bare silica or neutral capillary on a P/ACE 5510 apparatus (Beckman Coulter, Fullerton, CA) equipped with a UV absorbance detector. The working wavelength selected was 214 nm. Benzyl alcohol was used as an EOF marker. Capillaries were 27 or 37 cm in total length (20 or 30 cm to detector) with i.d. of 50 μm. Voltage within the linear range of Ohm plots were used. (Beyond this range Joule heating becomes a problem.) Samples were dialyzed overnight against the running buffer. Capillaries were rinsed at 20 psi for 2 min with deionized water and 5 min with running buffer before each run. A 2–4-s hydrodynamic sample injection time at 0.5 psi was used. The mobility (μ) was calculated by plotting sample velocity (V_{EOF} subtracted from the apparent sample velocity) as a function of field strength (Fig. 1). The slope of a linear least-squares fit of this plot is the sample mobility, for which precision is reported as the error of the slope. This procedure provides a better assessment of the accuracy of the mobility than single field calculations. While the precision of the mobility calculated by this method is ~10%, the reproducibility of the mobility at any given field is within 0.69–4.43%, which is in the range of typically reported CE errors [4,32,33]. The CE effective charge was calculated from the relation:

$$z_{\text{eff}} = \frac{\mu k_B T}{D_t e} \quad (1)$$

Table 1
pK_a values of charged residues

Residue	pK_a
Set 1	
Glu5	3.8
Asp10	0.4
Glu11	5.4
Asp20	3.6
Glu22	3.8
His31	9.05
Glu45	3.8
Asp47	3.0
Asp61	3.6
Glu62	2.9
Glu64	4.4
Asp70	0.5
Asp72	3.4
Asp89	4.0
Asp92	2.5
Glu108	4.6
Asp127	3.4
Glu128	3.7
Asp159	3.4
Arg	12
Lys	12
Tyr[a]	–
Cys[a]	–
N-term	7.35
C-term	3.9
Set 2	
Asp70	0.5
His31	9.1
Asp	3.9
Arg	12.5
Cys	8.3
Glu	4.2
Lys	10.5
Tyr	10.1
N-term	7.3
C-term	3.9
Set 3	
Asp70	0.5
His31	9.1
Asp	4.5
Arg	12.0
Cys	9.3
Glu	4.6
Lys	10.4
Tyr	9.7
N-term	7.3
C-term	3.9

[a] Cys and Tyr are not considered titratable in this set.

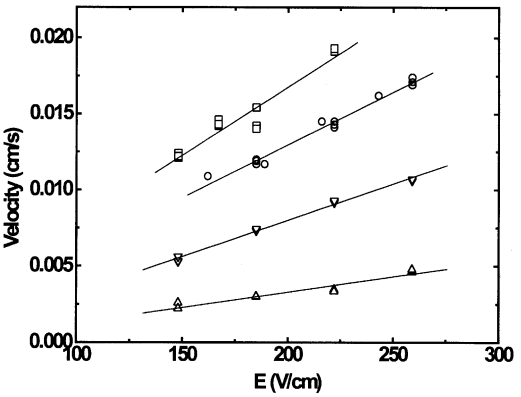

Fig. 1. CE velocity vs. *E*. Capillary electrophoresis (CE) of [*open squares*] WT ($N=15$), [*open circles*] SM ($N=14$), [*inverted open triangles*] DM ($N=12$), and [*open triangles*] TM ($N=12$) in 10 mM BTP, 100 mM KCl, pH 7.5 (20 °C). *N* is the number of measurements.

where *e* is the elementary charge, D_t is the translational diffusion coefficient, k_B is Boltzmann's constant and T is the absolute temperature. In capillary electrophoresis, the primary quantity determined by experiment is μ. This combined with a measurement of D_t yields z_{eff}. However, in the MCE measurements discussed later, the primary quantity determined by experiment is z_{eff}.

2.5. Dynamic light scattering

A Protein Solutions DynoPro was used to measure the hydrodynamic radius (R_h) of the proteins. Experiments were carried out at 20 °C in 10 mM BTP, 100 mM KCl, pH 7.5. The average resulting T4 radius from three experiments, 2.07 nm, was used to calculate the translational diffusion coefficient of $10.37\pm0.56\times10^{-7}$ cm^2 s^{-1} (95% confidence interval assuming no error in viscosity of 1 cps).

2.6. Analytical ultracentrifugation

Sedimentation velocity experiments were conducted using a Beckman Coulter XLA analytical ultracentrifuge. Data were acquired at 60 000 rev. min^{-1}, 20 °C, in 10 mM BTP, 100 mM KCl, pH 6.5, using absorbance detection. Loading concentrations were 1.22, 0.38 and 0.22 mg ml^{-1} as determined from best fit A_{280} values (analysis program: SEDFIT) using an extinction coefficient of 1.28 ml mg^{-1} cm^{-1} and a pathlength of 1.2 cm. No concentration dependence was observed. The concentration difference across an MCE cell is approximately five-fold and in this range. It was therefore assumed D_t is unchanged across the MCE cell. The partial specific volume ($\bar{v}$) used in fitting was 0.74 g ml^{-1} [34]. Fits of the data using SEDFIT [35] gave an average sedimentation coefficient (s) of 1.94 ± 0.06 s and an average translational diffusion coefficient of $10.20\pm0.71\times10^{-7}$ cm^2 s^{-1} (95% confidence interval for both). This D_t value was used in subsequent calculations of mobility and in BE modeling. In addition, D_t was calculated using the sedimentation velocity data along with sedimentation equilibrium data using the equation $D_t = sRT/M_b$, where R is the gas constant and M_b is the buoyant molar mass determined from $M_b = \sigma RT/\omega^2$ [36]; σ is the exponential coefficient for the concentration gradient in the analytical ultracentrifuge and ω is the angular velocity. This method circumvents uncertainty associated with $\bar{v}$ and gives a diffusion coefficient within error of the above value ($10.16\pm0.57\times10^{-7}$ cm^2 s^{-1}). Data were edited using WINREEDIT and analyzed using WINNONLIN (both programs are available at ftp://alpha.bbri.org/rasmb/spin).

2.7. Membrane-confined electrophoresis

The MCE instrument has been described previously [24,25,37]. Briefly, macro-ions are confined in a small $2\times2\times4$-mm^3 quartz cuvette, with the ends sealed with semi-permeable membranes. An electric field is established between the membranes, and the formation of a steady-state gradient of the macro-ions is monitored using an imaging spectrophotometer. A buffer flow of 10 ml h^{-1} past the analysis chamber provides constant solvent conditions for electrophoresis. Experiments were conducted at a controlled temperature of 20.0 ± 0.1 °C using 16 μl of a solution containing 1.5–2.5 mg ml^{-1} protein.

Recent research has demonstrated that concentration gradients may develop for small anions, most likely due to residual carboxyl groups on the membranes capping the analysis chamber, and a test for this has been developed using NO_3^- to allow monitoring of the anion at 300 nm. Tests reveal that under the conditions of the experiments reported here, no such gradients are observed. It was assumed that the Cl^- used in the MCE experiments behaves similarly.

Once it was demonstrated that the steady-state distributions were not affected by bulk solvent flow or small ion gradients, σ was determined by non-linear least-squares analysis using the combined data from all fields normalized to the lowest field [25].

2.8. Determination of mobility (μ) from steady-state measurements

At steady state, the flux due to the electrophoresis of a membrane-confined species is exactly balanced by the flux due to its diffusion at each point in the system [38]. The result is that all system properties, including the concentration gradient of any membrane-confined species, are invariant with time. Thus, SSE is analogous in many respects to equilibrium sedimentation.

For a system with a single macro-ion species, the equation describing the macro-ion concentration gradient at steady state is:

$$c = a_o e^{\sigma(x-x_0)-2B^*Mc} \quad (2)$$

where x is the position in cm; x_0 is the arbitrary reference position; c is the macro-ion concentration at x; $a_0 = c_0 e^{2B^*Mc_0}$, where c_0 is equal to c at x_0; σ, in units of cm^{-1}, is the exponential coefficient that characterizes the steady-state concentration gradient in the limit as c approaches zero; M is the molar mass, in g mol^{-1}, of the macro-ion; and B^* is the apparent second virial coefficient that accounts for the apparent influence of c on the exponent of Eq. (2) [39]. That influence can include, but *is not limited to*, the effect that c has on the thermodynamic non-ideality of the system. For example, a shallow gradient in the small, mobile ions will result in a shallow gradient in the electric field. This may alter the macro-ion concentration distribution in a manner analogous to the effects of thermodynamic non-ideality. Fitting data to a model that includes B^* allows for such a gradient and improves the accuracy of the determination of σ.

The time needed for the concentration distribution to reach steady state (generally 8–9 h) was judged using MATCH (courtesy of David Yphantis, available at the RASMB archive: ftp://www.bbri.org/rasmb). Absorbance readings were truncated at each end to remove points distorted by reflections from the membranes. Non-linear least-squares analysis was used to determine σ [25,40,41]. For each mutant, σ was determined for a minimum of five fields. In all cases, the data adequately fitted to a model consisting of a single, non-ideal species (i.e. B^* non-zero). Diagnostic graphs of σ as a function of the electric field, E, and σ/E as a function of E were constructed to test for bulk solvent flow [25]. Tests for bulk fluid flow were also conducted using the neutral molecule rhodamine dextran as previously described [25].

The dimensionless effective charge is related to σ appearing in Eq. (2) by the relation:

$$z_{\mathrm{eff}} = \frac{k_B T \sigma}{Ee} \quad (3)$$

where all quantities have been previously defined. (Since E is typically in V cm^{-1}, two useful unit identities are: 1 esu = 300 V cm, and 1 erg = 1 esu^2 cm^{-1}.) In MCE, it should be emphasized that z_{eff} is the primary quantity derived from experiment and not μ. Given z_{eff} and D_t, μ can be calculated from Eq. (1).

The effective charge measured by MCE depends on the properties of the system and is affected by ion flows (i.e. the electrophoretic effect and ion relaxation). Thus, z_{eff} is a system parameter. Although z_{eff} is not a molecular parameter, it is the natural parameter obtained from the analysis of SSE data and is analogous to the buoyant molar mass, M_b, in equilibrium sedimentation.

2.9. Boundary element (BE) modeling

The protein is modeled as a low-dielectric (dielectric constant ε_i) solid of arbitrary shape with

an arbitrary charge distribution within that encloses the hydrodynamic shear surface S_p. The solvent (dielectric constant ε_o) is represented as an incompressible Newtonian fluid of viscosity η. The usual 'stick' boundary condition is assumed to apply, which states that the velocity of the model protein and that of the fluid match on S_p. The co- and counterions are treated at the continuum level in the fluid and are assumed to obey the Poisson equation:

$$\nabla\cdot(\varepsilon(\mathbf{x})\nabla\Lambda(\mathbf{x})) = -4\pi\rho(\mathbf{x}) \tag{4}$$

where $\mathbf{x}$ is a point in space, and ρ, ε and Λ are the local charge density, dielectric constant and electrical potential, respectively. The motion of the polyion is assumed small enough so that the local fluid velocity, $\mathbf{v}$, and pressure, p, are described by the linearized Navier–Stokes and solvent incompressibility equations:

$$\eta\nabla^2\mathbf{v}(\mathbf{x}) - \nabla p(\mathbf{x}) = -\mathbf{s}(\mathbf{x}) \tag{5a}$$

$$\nabla\cdot\mathbf{v}(\mathbf{x}) = 0 \tag{5b}$$

where $\mathbf{s}$ is the local external force per unit volume acting on the fluid. When the external forces in the fluid arise from equilibrium charge interactions, as well as charge interactions with external electric fields, then $\mathbf{s}(\mathbf{x}) = -\rho(\mathbf{x})\nabla\Lambda(\mathbf{x})$.

If ion relaxation is ignored, then the equilibrium ion distributions can be used and Eq. (4) reduces to the Poisson–Boltzmann equation. In this limiting case, Eq. (4) becomes uncoupled from Eqs. (5a) and (5b) and it is possible to solve Eq. (4) either analytically in certain limiting cases, or numerically [42]. These results can then be used to solve the velocity and pressure fields [Eqs. (5a) and (5b)]. This was the strategy employed by Henry in solving for the electrophoretic mobility of spherical polyions with centrosymmetric charge distributions in the absence of ion relaxation [22]. In addition, this approach has been used to investigate the electrophoretic mobility of other model structures, such as prolate and oblate ellipsoids [43], spherical polyions containing non-centrosymmetric charge distributions [44], and structures of arbitrary shape and charge distribution [45]. To include the effects of ion relaxation in the steady-state transport of a model polyion, it is also necessary to solve an ion transport equation for each mobile species, α, of valence z_α, present:

$$\nabla\cdot\mathbf{j}_\alpha(\mathbf{x}) = 0 \tag{6a}$$

$$\mathbf{j}_\alpha(\mathbf{x}) = n_\alpha(\mathbf{x})\mathbf{v}(\mathbf{x}) - D_\alpha\left(\nabla n_\alpha(\mathbf{x}) + \frac{ez_\alpha n_\alpha(\mathbf{x})}{k_B T}\nabla\Lambda(\mathbf{x})\right) \tag{6b}$$

where $\mathbf{j}_\alpha$ is the local current density, n_α is the local number density and e is the elementary charge. At this level, Eqs. (4), (5a), (5b), (6a) and (6b) are coupled together and must be solved simultaneously. Their solution to determine electrophoretic mobilities of spheres [6–9], long cylinders [10,11], and particles of arbitrary shape and charge distribution [16–20] have been reported.

The BE numerical procedure is outlined only briefly in the present work. Eqs. (4), (5a), (5b), (6a) and (6b) are solved iteratively until convergence of all of the various fields is achieved. Then, the total force, $\mathbf{f}$, exerted by the model polyion on the fluid is computed. Two distinct transport cases must be considered. In Case 1, the polyion is translated with velocity $\mathbf{u}$ through an otherwise stationary fluid in the absence of an external electric field. By translating the model along three orthogonal directions, it is straightforward to determine the nine components of the translational friction tensor, $\underline{\Xi}_t$, by the relation:

$$\mathbf{f}^{(1)} = \underline{\Xi}_t\cdot\mathbf{u} \tag{7}$$

where the superscript (1) denotes Case 1. In Case 2, the polyion is held stationary in a fluid that is at rest far from the particle, but it is subjected to a constant external field, $\mathbf{E}$. In this case, a tensor, $\mathbf{Q}$, analogous to $\underline{\Xi}_t$ can be determined from the forces along three orthogonal field directions:

$$\mathbf{f}^{(2)} = -\underline{\mathbf{Q}}\cdot\mathbf{E} \tag{8}$$

We can view $-\mathbf{f}^{(2)}$ as the force acting on a polyion that is fixed in space by a tether. This occurs, for example, when a polyion is entrapped in a gel [46,47]. Thus, $\mathbf{Q}$ is sometimes referred to as a 'tether force tensor' [20]. Another interpretation can be made by considering the special case of a weakly charged polyion at very low salt. In this case, $\mathbf{Q}\rightarrow\mathbf{QI}$, where $\mathbf{I}$ is the 3×3 identity

tensor and **Q** is the formal charge on the polyion (the bare charge of the macro-ion plus any solution charge that is entrapped within S_p). At finite salt concentration, however, **Q** does not correspond to the actual charge of the polyion due to the coupled influences of polyion charge distribution, shape, solvent and mobile salt on $\mathbf{f}^{(2)}$. Thus, **Q** is sometimes referred to as an 'effective charge tensor' [20]. Undoubtedly, the effective charge, Q_{eff}, represents an isotropic average over the components of **Q** in general, but this subject needs further study.

To a good approximation, $\underline{\Xi}_t$ is related to the translational diffusion constant, D_t, by the relation:

$$D_t \approx \frac{k_B T}{3} \mathrm{Tr}(\underline{\Xi}_t^{-1}) \tag{9}$$

where Tr denotes the trace (summing of diagonal components). To be precise, it is necessary to compute D_t relative to a particular body-fixed origin called the 'center of diffusion' [48]. Nonetheless, Eq. (9) is accurate in most cases provided a reasonable choice of body-fixed origin is made [49]. At sufficiently weak external field where no significant orientation of the particle occurs, the average electrophoretic mobility of the particle, μ, is given by:

$$\mu = \frac{1}{3} \mathrm{Tr}(\underline{\Xi}_t^{-1} \cdot \underline{Q}) \tag{10}$$

where the -1 superscript denotes inverse. The procedure used to construct detailed models of T4 lysozyme and its mutants has been described in detail previously [45]. The non-hydrogen coordinates of wild type T4 [2LZM] and SM [1L44] were obtained from the Protein Data Bank. Associated with each non-hydrogen atom is an atom 'exclusion radius', δ_1, which is assumed constant for all atoms. Plated structures consisting of interconnected triangular platelets are then constructed to completely enclose the protein. Fig. 2 shows a schematic of wild type T4 along with the plated structure, which represents the hydrodynamic shear surface, S_p. Let N denote the number of platelets representing the protein surface. Although each triangular platelet is defined by three vertex vectors, a single vertex vector is common to several

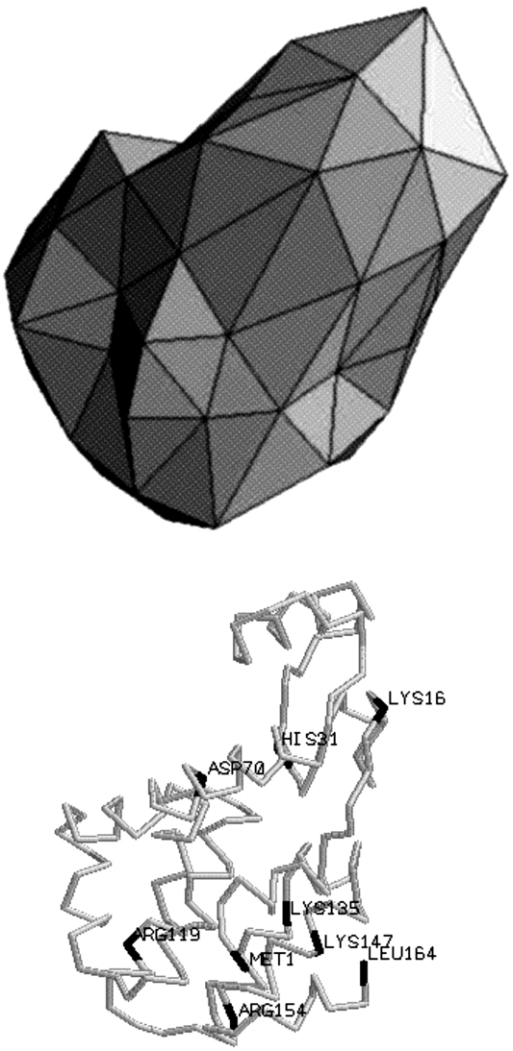

Fig. 2. T4 lysozyme models. The top structure is a 128-plate model depicting the hydrodynamic shear surface, S_p, of the protein. The ribbon model below denotes the backbone structure of T4 along with the positions of some of the key residues.

platelets, and the number of distinct vertex vectors actually equals $N/2+2$. The placement of each vertex vector is determined by progressively moving outward from a common origin and stopping at a large number of points. At each point, all of the atoms are scanned for possible overlap. The last point (moving outward) at which overlap occurs is taken to be the endpoint of that vertex vector. This procedure is repeated for each vertex

Table 2
Summary of T4 lysozyme mobility

T4 lysozyme	Mobility $\times 10^5$ ($cm^2\ V^{-1}\ s^{-1}$)		
	μ_{CE}	μ_{SSE}	μ_{BE}[a]
WT	8.94 ± 0.70	9.34 ± 0.66	9.39 ± 0.28
SM	6.93 ± 0.30	6.42 ± 0.45	6.80 ± 0.21
DM	4.78 ± 0.13	4.72 ± 0.35	4.89 ± 0.15
TM	2.01 ± 0.17	1.81 ± 0.13	2.24 ± 0.09
QM	Migrated with EOF	No gradient formed	–

Experimental mobility obtained by: μ_{CE}, capillary electrophoresis; μ_{SSE}, steady-state electrophoresis; and μ_{BE}, boundary element modeling.

[a] μ_{BE} calculated using BE formal charges and includes IR.

vector in order to generate S_p. For a particular choice of δ_1, the resulting structure, S_p, is used in a Case 1 transport study to first determine the translational friction tensor, Ξ_t [Eq. (7)], and then the translational diffusion constant, D_t [Eq. (9)]. From experiment, D_t for wild type T4 in water at 20 °C is known to be 10.2×10^{-7} $cm^2\ s^{-1}$ and that value is used to define δ_1 in our modeling.

In addition to the surface S_p, it is also necessary to subdivide the volume of fluid surrounding the polyion, V, into discrete volume elements and compute the external force, **s**, fluid velocity, **v**, and other field quantities within those volume elements. In the BE methodology, the approximation is made that field quantities do not vary over a particular platelet of S_p, or within a particular volume element of V [16]. By carrying out a series of calculations on models with increasing N, it is straightforward to extrapolate to the continuum ($N \rightarrow \infty$) limit [18]. The procedure followed in the present work is to generate a series of M 'shells', with the innermost shell corresponding to S_p. Typically, $M = 50$ and each shell is made up of N platelets. The volume between successive shells is then divided into N volume elements, which resemble truncated pyramids. To generate successive shells, a procedure very similar to that used to generate S_p is employed, except a larger atom exclusion radius is used. Let δ_j denote the atom exclusion radius for the j-th shell. Because field quantities vary most strongly near S_p and more slowly far from S_p, it is desirable to gradually increase the distance between successive shells as j increases. This is accomplished by writing $\delta_{j+1} = \delta_j(1+\beta)$, where β is a small, positive constant to be determined. It then follows that the total thickness of the solvent layer external to polyion that is included is approximately $T = \delta_M - \delta_1 = \delta_1[(1+\beta)^{M-1} - 1]$. Past work has shown that, provided T is greater than or equal to $12/\kappa$, where κ^{-1} is the Debye–Hückel screening length, then electrophoretic mobilities become independent of T to a good approximation [18]. For an aqueous solvent in monovalent salt at 20 °C, κ (in $Å^{-1}$) $= 0.3277 I^{1/2}$. Thus, we set $T = S/\kappa$, where S is typically 12 or 16, and this is used to define β.

In addition to the surface topography of the proteins, another important requirement for realistic modeling in the present work is their detailed charge state. In the present work, the charge of a particular amino acid residue is estimated from the pK_a of the particular residue. From the work of E. Anderson, the pK_a values of all of the Glu and Asp residues of wild type T4 lysozyme have been determined at 10 °C at an ionic strength of approximately 0.11 M, and those values are used in the present work. The pK_a of His31 is well known [31]. For the C-terminus and N-terminus, average values typical of many known proteins are used [29,30]. Finally, the pK_a values of the Lys and Arg residues are taken to be 12.

Since the experiments are carried out at pH 7.5, considerable uncertainty in the pK_a of a particular residue does not lead to significant error in the resulting residue charge, unless the pK_a lies between approximately 6.5 and 8.5. Since the pK_a values were measured at a temperature 10 °C lower than the conditions of the CE and MCE

measurements, some comments on the temperature dependence of the acid dissociation constants are appropriate. It is straightforward to estimate changes in a residue pK_a from the corresponding ionization enthalpies using the Gibbs–Helmholtz equation [50]. A carboxylic acid residue, for example, has an ionization enthalpy of approximately 2.5 kcal mol^{-1} [51]. Using this value, it is straightforward to estimate a pK_a change of -0.064 when the temperature is raised by 10 °C. Because these corrections are small and because of other uncertainties and assumptions of modeling, the uncorrected pK_a values were used in the present work. We have also assumed that the pK_a values for identical residues in the different mutants are unchanged, despite the difference in net charge on each mutant protein. All of these considerations lead to some uncertainty in the absolute value of the formal charge. However, for the mutants used in this study, Lys and Arg have been replaced by Glu or Asp, and the pK_a values of all these residues fall outside the range 6.5–8.5. Accordingly, while the formal charge on any particular mutant is difficult to determine, the charge change from one mutant to another is better defined.

3. Results

3.1. Mobility (μ) of T4 lysozyme

The mobility results are given in Table 2. As an independent means of assessing SSE results, capillary electrophoresis was used. Also included in Table 2 are BE model results (that include ion relaxation and account for the detailed charge distribution within the proteins). As Table 2 shows, CE experimental results are in good agreement with those from SSE. Fig. 3 shows that ratios of experimental mobilities to BE predictions do track well with formal charge for WT, SM and DM, but not for TM. In the latter cases we observe a significantly greater drop in observed mobility with decreased formal charge.

3.2. BE modeling results

The results of detailed BE modeling with and without inclusion of ion relaxation are shown in

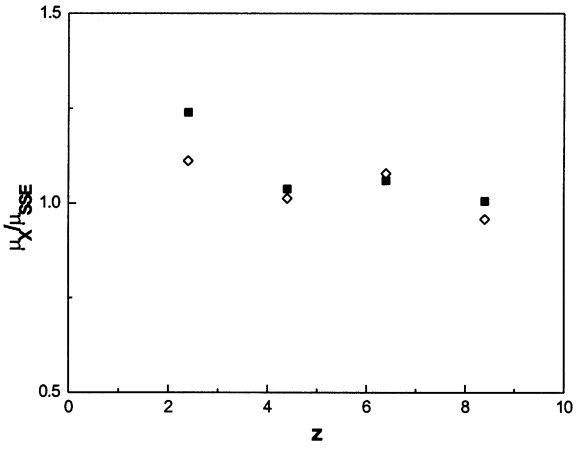

Fig. 3. Mobility ratios. μ_{CE}/μ_{SSE} [*open diamonds*] and μ_{BE}/μ_{SSE} [*filled squares*] vs. z for WT, SM, DM and TM at 10 mM BTP, 100 mM KCl, pH 7.5 (20 °). μ_{SSE} was obtained by fitting Eq. (2) with B^* non-zero and μ_{BE} includes ion relaxation.

Fig. 4. Account is taken of the detailed charge distribution within the model proteins. For BE studies, it is necessary to know the small ion mobilities or diffusion constants [the D_α in Eq. (6b)]. These are related to the hydrodynamic radii, r_α, of the small ions by the Stokes–Einstein formula, $D_\alpha = k_B T/6\pi\eta r_\alpha$, which in turn are related to the limiting molar conductivity of the small ions, λ_α^∞ (at 25 °C in 10^{-4} S m^2 mol^{-1}) by:

$$r_\alpha = 92.01\frac{z_\alpha^2}{\lambda_\alpha^\infty} \tag{11}$$

where r_α is in Å and z_α is the valence of the ion. For K^+, Cl^- and BTP^+, $r_2 = 1.252$, 1.206 and 3.456 Å, respectively. The limiting molar conductivity values of simple ions can be found in standard references [52]. The limiting molar conductivity of BTP^+ has been measured in our lab (J. Durant and T. Laue) and found to be $26.95 \pm 0.56 \times 10^{-4}$ S m^2 mol^{-1} at 25 °C.

In the BE modeling, most models consisted of 128 plates, and mobility values reported either represent the average of nine independent model structures, or else a structure that yields a mobility closest to the average mobility was employed. Several models consisting of 512 plates were also examined and the resulting mobility values agreed

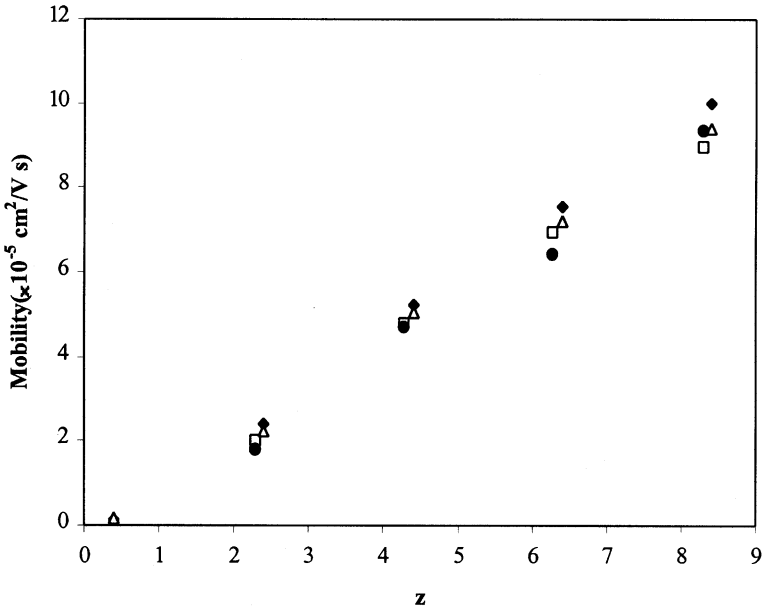

Fig. 4. Effect of ion relaxation on boundary element modeling and comparison with experiment: [*diamonds*] BE without ion relaxation, [*open triangles*] BE with ion relaxation, [*filled circles*] SSE (experiment), [*open squares*] CE (experiment).

with the simpler 128 plate results to an accuracy of several percent. Since this accuracy was comparable to the variation observed between different 128 plate structures, and since computation time varies approximately as the square of the number of plates comprising the structure, it was felt that the 128 plate structures represented a good compromise between realism/accuracy and practicality. As Table 3 and Fig. 4 show, the detailed models are in excellent agreement with experimental results for WT, SM and DM, particularly when ion relaxation is included.

The details of the charge distribution influence the mobility and, by extension, z_{eff}/z. Even the mobility of a spherical polyion in the absence of ion relaxation depends on the variation in electro-

Table 3
Experimental and model-predicted charge of T4 lysozyme

T4	Average z[a]	BE z	Effective charge z_{eff} (proton equivalents)					z_{eff}CE/ z_{eff}SSE	z_{eff}BE/ z_{eff}SSE
			CE	SSE	DHH	Booth	BE[b]		
WT	8.281±0.364	8.402	2.214±0.231	2.311±0.202	2.66	2.50	2.325	0.958	1.006
SM	6.281±0.364	6.402	1.715±0.140	1.589±0.070	2.01	1.95	1.684	1.079	1.060
DM	4.281±0.364	4.402	1.182±0.088	1.167±0.114	1.37	1.35	1.211	1.013	1.038
TM	2.281±0.364	2.402	0.498±0.055	0.448±0.023	0.73	0.73	0.555	1.112	1.239
QM	0.281±0.364	0.402	–	–	0.09	0.09	0.041	–	–

z_{CE}, charge calculated by Eq. (1) from capillary electrophoresis experiments; z_{SSE}, charge determined by steady-state electrophoresis experiments; z_{DHH}, charge predicted by Debye–Hückel–Henry theory using Eq. (12); z_{Booth}, charge predicted by Booth using Eq. (13); z_{BE}, charge predicted by boundary element modeling by Allison.

[a] The average formal charges were calculated from three sets of pK_a values as described in Section 2. The error is estimated for the 90% confidence level.

[b] Includes IR.

Table 4
Effects of charge distribution

Mutant	z	z_{eff}BE	z_{eff}BE/z
TM (R119E/K135E/K147E)	2.402	0.555	0.231
TM1 (R16E/K135E/K147E)	2.402	0.701	0.292
TM2 (K16E/R119E/K135E)	2.402	0.608	0.253

static potential over its surface, and not simply the average electrostatic surface potential [15]. With this in mind, BE studies on several additional models have been carried out to address this question of the influence of charge distribution on z_{eff}/z. In T4 mutant species TM (R119E/K135E/K147E), all of the mutated residues are in the same domain of the protein. In the hypothetical species TM1 (K16E/K135E/K147E) and TM2 (K16E/R119E/K135E), the three mutated residues are in different protein domains. Shown in Table 4 are the z_{eff}/z ratios for these three species. For the three TM model proteins, there is clearly considerable variation in the charge ratios, which is due to the details of the charge distribution within the protein. Species TM1 with charge mutations in both protein domains has a z_{eff}/z similar to what is observed in species DM, SM and WT. In addition, if the charge is reduced even further, as in the QM species, even greater deviation in z_{eff}/z from the high charge value is observed.

3.3. Effective charge of T4 lysozyme

Accurate measurement of the effective charge by MCE requires: (1) that the concentration profile fits well to a model consisting of a single species; (2) that σ increases linearly with the applied field (E); and (3) there are no contributions to σ from bulk solvent flow [25].

Fig. 5 shows that at a given field, the steady-state concentration gradient across the cell is unique for each charge mutation and that these profiles can be adequately fitted (Fig. 5 inset) to an exponential as given by Eq. (2). As might be expected, superior fits are obtained when the expression includes contributions to the profile due to apparent non-ideality, given by the term B^*. Crystallographic data and stability studies [26], as well as sedimentation velocity experiments, indicate that these charge mutants are otherwise identical with respect to tertiary structure and hydrodynamic properties.

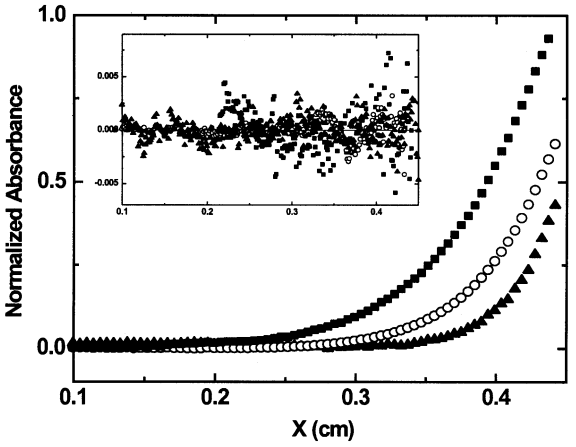

Fig. 5. MCE steady-state concentration gradients. Specific cases include: [*filled triangles*] WT (σ = 34.773 cm^{-1}), [*open circles*] SM (σ = 25.242 cm^{-1}), and [*filled squares*] DM (σ = 19.972 cm^{-1}) all at a field strength of 0.4 V cm^{-1} in 10 mM BTP, 100 mM KCl, pH 7.5 (20 °C).

As can be observed in Fig. 6a, σ does vary linearly with E. Linear fits give intercepts of within error of zero, indicating there is no significant field-independent bulk fluid [25]. A more sensitive test for both the linearity and bulk fluid flow is

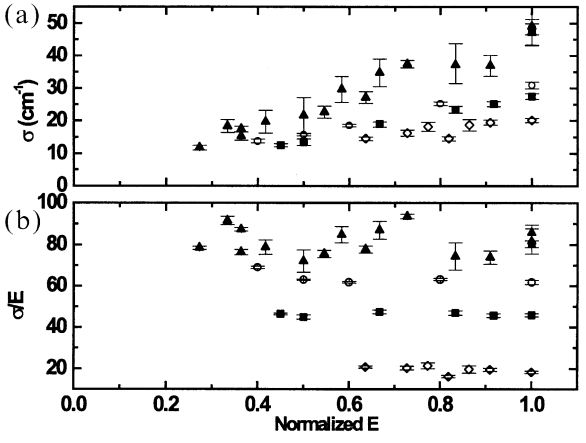

Fig. 6. (a) σ vs. applied field, E. Specific cases include: [*filled triangles*] WT, [*open circles*] SM, [*filled squares*] DM, and [*filled diamonds*] TM; in 10 mM BTP, 100 mM KCl, pH 7.5 (20 °C). (b) σ/E vs. E.

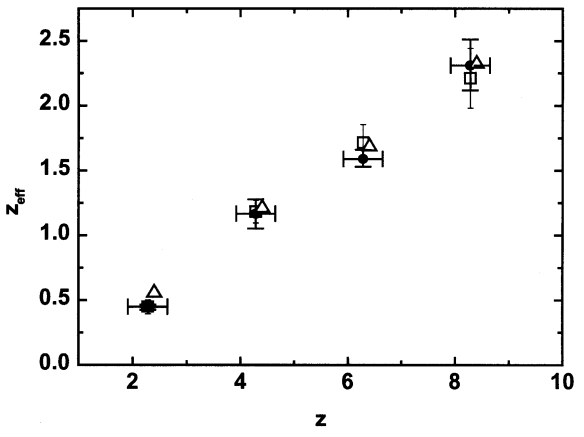

Fig. 7. Effective charge as a function of formal charge. Cases include: [*filled circles*] SSE, [*open squares*] CE, and [*open triangles*] BE results. SSE: slope 0.30 ± 0.02, y intercept -0.21 ± 0.12. CE: slope 0.29 ± 0.02, y intercept -0.15 ± 0.11. BE: slope 0.29 ± 0.12, y intercept -0.12 ± 0.07. The confidence intervals are 90% for the x-axis and 95% for the y-axis.

obtained from a graph of the ratio of σ/E vs. E (Fig. 6b). The lack of any systematic deviation of σ/E with E indicates a lack of charge heterogeneity, and shows that the data are unaffected by bulk solvent flow dependent on E^n, for $n \neq 1$ (i.e. non-electroosmotic flow) [25].

Table 3 and Fig. 7 summarize the effective charge results from SSE and CE experiments and BE modeling. With regards to the BE modeling, effective charges are related to mobility and the translational diffusion constant by Eq. (1). As is expected from theory, the effective solution charge is substantially less than the formal charge [12,53] and does track changes in the formal for charges in the range from $+4$ to $+9$. Boundary element predictions, as well as experimental CE and SSE results, show that the ratio of effective charge to formal charge is nearly constant, except for the case of TM. Wall interactions and the difficulty in fitting low-curvature data may explain why CE and SSE, respectively, both give values slightly lower than that predicted by BE.

4. Discussion

Use of T4 WT and charge mutants allowed us to cover a more extensive charge range within a single set of experimental conditions than could be accomplished with pH changes. The differing response to the electric field is then solely attributed to the change in charge due to amino acid replacements, and not to changes in the shape. Similar experiments carried out by changes in pH would be limited, in that multiple buffers would be needed to cover as substantial a range in charge, introducing additional uncertainties and, at the extremes, some changes in protein frictional drag that would be expected as denaturing pH values were approached. By looking at a series of charge mutants of a single protein, these concerns have been eliminated. In analyzing the mobility and charge of the various charge mutants of T4 bacteriophage lysozyme, several models are considered in order of increasing complexity and realism.

In the absence of ion relaxation, the effective charge of a spherical model macro-ion containing a centrosymmetric charge distribution of total charge Q is given by [38,54]:

$$Q_{\text{eff}} = Q\frac{f(\kappa a)}{(1+\kappa a)} \qquad e\varsigma/k_{\text{B}}T \ll 1 \tag{12}$$

where f, a function of κa, is Henry's function, ς is the macro-ion surface potential (zeta potential) and a is the radial distance out to the surface of shear [21,38,54], which is taken in this work to be the sum of the Stokes radius of T4 and Cl^-. For the work presented here, $\kappa a = 2.36$, $f(\kappa a) = 1.08$ and $a = 2.197$ nm. Henry's function accounts for electrophoretic effects. Note that there is a larger error associated with the calculation of Q than the measurement of Q_{eff}, and thus typical least-squares analysis is in reality not valid. The Debye–Hückel–Henry (DHH) expression given by Eq. (12) assumes the validity of the linear Poisson–Boltzmann relation in describing the ion distribution around the macro-ion and should be valid at low surface potentials. As our results show, when the surface potential approaches 20 mV, as in the case of WT ($k_{\text{B}}T = 25$ mV), Q_{eff} from Eq. (12) is within 15% of experimental SSE values and 20% of CE values. If we consider all the SSE data, the slope of Q_{eff} as a function of formal charge is within 7% of the predicted slope [0.321 predicted by Eq. (12)]. In all cases, as

expected, the approximation yields higher values than those obtained experimentally.

Examination of our results in the context of Booth's work [7] shows better agreement. This model extends the Debye–Hückel–Henry model discussed above by including the effects of ion relaxation to lowest order. Booth's equation, as given by Tanford [50] (Eqs. 24–26, p. 416), can be written as:

$$Q_{\text{eff}} = Q\frac{f(\kappa a)}{(1+\kappa a)} + \sum_{j=2}^{\infty} Q^j \frac{e^{j-1}}{a^{j-1}(\varepsilon k_B T)^{j-1}} \times (X_j(\kappa a;q) + Y_j(\kappa a;q) + Z_j(\kappa a;q;q^*)) \quad (13)$$

where X, Y and Z are complex functions that attempt to include ion relaxation effects [7,50,55]. From Eq. (13) we find the values for Q_{eff} that are within 8% (SSE) and 13% (CE) for WT. If we again compare the slope of Q_{eff} vs. Q with that predicted by Booth's equation, the match is within 1% of SSE.

If we make use of the boundary element model developed by Allison and co-workers, we observe that the predictive discrepancy for WT is $<1\%$ (SSE) and 5% (CE). The same trend is observed throughout the data. Although the experimental slope of Q_{eff} vs. Q is 4% greater than BE predicts, the *individual values* track much closer to those predicted by BE than any of the other models. These results are summarized in terms of z_{eff} and z in Fig. 8 and Table 3 (recall $Q_{\text{eff}} = z_{\text{eff}}e$). The predictive ability of BE is particularly apparent if we now examine the behavior of the lower charged mutants. Both SSE and CE show that the z_{eff}/z ratio drops by approximately 20% for TM, and most likely even more for QM (since no gradient or mobility was experimentally observed for QM). Although neither Debye–Hückel–Henry theory nor the more complex work of Booth predicts this, BE modeling does. The results suggest that mobility is sensitive to the charge distribution for structures with many charged groups but of low net charge. The model predicts that if the three charge mutations of TM are repositioned such that the protein still has the same formal charge, the z_{eff}/z ratio changes from 0.23 (TM) to 0.29 (K16E/K135E/K147E) to 0.25 (K16E/R119E/K135E). If z is reduced even further, as in the QM species, even greater deviation in z_{eff}/z from the high charge value is predicted. In the limit of a pure quadrupolar charge distribution with $z=0$, model studies show that the mobility is not necessarily zero [15,16]. Thus, the commonly held assumption in biophysics that the isoelectric point and the point of zero mobility are the same is not strictly correct. Indeed, there is evidence in early literature [56,57] that suggests that there may be a significant discrepancy between these two points, and that the discrepancy becomes greater as the ionic strength increases.

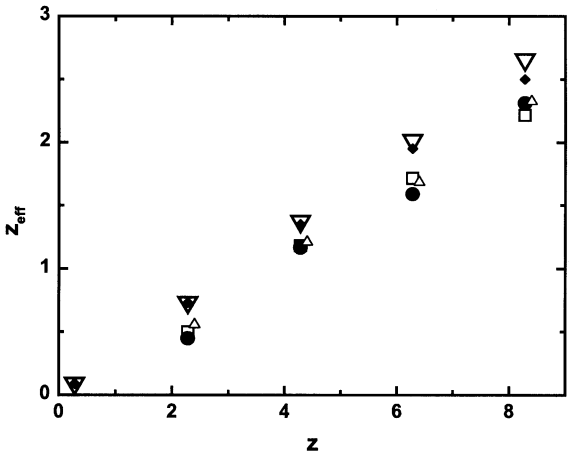

Fig. 8. Effective charge as a function of formal charge II. Cases include: [*inverted open triangles*] DHH, [*filled diamonds*] Booth, [*filled circles*] SSE, [*open squares*] CE, and [*open triangles*] BE results. DHH: slope $0.32 \pm 4.18 \times 10^{-17}$, y intercept $0 \pm 2.14 \times 10^{-16}$. Booth: slope 0.30 ± 0.01, y intercept 0.03 ± 0.03. SSE: slope 0.30 ± 0.02, y intercept -0.21 ± 0.01. CE: slope 0.29 ± 0.02, y intercept -0.15 ± 0.11. BE: slope 0.29 ± 0.12, y intercept -0.12 ± 0.07.

Modeling a macro-ion as a sphere with a centrosymmetric charge distribution and possibly including the effects of ion relaxation yields, under certain conditions, mobilities and effective charges that are fairly accurate. However, detailed structural information combined with the electrostatic potential treated at the level of the full Poisson–Boltzmann equation, including ion relaxation, yields values in excellent agreement with experimental results (Fig. 8).

5. Conclusion

T4 lysoyzme was chosen for this work because it is a well-characterized, stable protein for which a series of charge mutants have been developed. Thanks largely to the extensive work of Matthews and co-workers [26], the structure and many other properties of T4 and its mutants are now well known. These characteristics make it an ideal macro-ion for work that combines experimental and modeling results to investigate electrophoretic processes. Steady-state MCE and CE results have been obtained over a wide range of charges with the use of T4 WT and mutants. MCE offers, as does CE, low sample consumption, but can cover a larger range of ionic strengths and does not have the drawback of capillary wall interactions.

The electrolyte chosen for this work was KCl. With this choice, the constituent small ions of the solvent have nearly identical transport properties, thus reducing electroosmotic flows to demonstrably negligible levels [25]. As has been shown, the electrophoretic mobilities measured agree, to within experimental uncertainty, with the values predicted by the boundary element model for the higher charged subset. While BE does predict a non-linear drop in mobility as the formal charge is diminished, the experimental results suggest the drop may be even more dramatic, which will naturally be a point of further investigation. Nonetheless, BE has been shown to be a powerful predictive tool. It should be noted that agreement between experimental results and those from modeling improves progressively as we: (a) include the detailed shape of the protein; (b) account for the detailed charge distribution; and (c) account for ion relaxation.

Acknowledgments

This work was funded by NSF grant MCB-9807550 (T.L.), American Heart Association grant 9650773N (T.L.) and NSF grant MCB-807541 (S.A.). The authors would also like to acknowledge Brian Matthews and Walter Baase for supplying the clones and for their much-appreciated advice on the protein purifications.

References

[1] Y.J. Yao, S.F.Y. Li, Determination of diffusion coefficients by capillary zone electrophoresis, J. Chromatogr. Sci. 32 (1994) 117–120.
[2] K.D. Cole, P. Todd, K. Srinivasan, B.K. Dutta, Free-solution electrophoresis of proteins in an improved density gradient column and by capillary electrophoresis, J. Chromatogr. A 707 (1995) 77–85.
[3] L. Mitnik, L Salome, J.L. Viovy, C. Heller, Systematic study of field and concentration effects in capillary electrophoresis of DNA in polymer solutions, J. Chromatogr. A 710 (1995) 309–321.
[4] N.C. Stellwagen, C. Gelfi, P.G. Righetti, The free solution mobility of DNA, Biopolymers 42 (1997) 687–703.
[5] P.G. Righetti, C. Gelfi, Capillary electrophoresis of DNA in the 20–500 bp range: recent developments, J. Biochem. Biophys. Methods 41 (1999) 75–90.
[6] J.T.G. Overbeek, Theorie der electrophorese. Der relaxationseffekt, Kolloid-Beih. 54 (1943) 287–364.
[7] F. Booth, The cataphoresis of spherical, solid, non-conducting particles in a symmetric electrolyte, Proc. R. Soc. Lond. A 203 (1950) 514–533.
[8] P.H. Wiersema, A.L. Loeb, J.T.G. Overbeek, Calculation of the electrophoretic mobility of a spherical colloid particle, J. Colloid Interface Sci. 22 (1966) 78–99.
[9] R.W. O'Brien, L.R. White, Electrophoretic mobility of a spherical colloid particle, J. Chem. Soc. Faraday Trans. 74 (2) (1978) 1607–1626.
[10] D. Stigter, Electrophoresis of highly charged colloidal cylinders in univalent salt solutions 1. Mobility in transverse field, J. Phys. Chem. 82 (1978) 1417–1423.
[11] D. Stigter, Electrophoresis of highly charged colloidal cylinders in univalent salt solutions. 2. Random orientation in an external field and application to polyelectrolytes, J. Phys. Chem. 82 (1978) 1424–1429.
[12] R.W. O'Brien, The solution of the electrokinetic equations for colloidal particles with thin double layers, J. Colloid Interface Sci. 92 (1983) 204–216.
[13] S.S. Dukhin, V.N. Shilov, Dielectric Phenomena and the Double Layer in Disperse Systems and Polyelectrolytes, John Wiley & Sons, New York, 1974.
[14] M. Fixman, Thin double layer approximation for electrophoresis and dielectric response, J. Chem. Phys. 78 (1983) 1483–1491.
[15] Y.E. Solomentsev, Y. Pawar, J.L. Anderson, Electrophoretic mobility of non-uniformly charged spherical particles with polarization of the double layer, J Colloid Interface Sci. 158 (1993) 1–9.
[16] S.A. Allison, Modeling the electrophoresis of rigid polyions. Inclusion of ion relaxation, Macromolecules 29 (1996) 7391–7401.
[17] S.A. Allison, M. Potter, J.A. McCammon, Modeling the electrophoresis of lysozyme. II. Inclusion of ion relaxation, Biophys. J. 73 (1997) 133–140.

[18] S.A. Allison, S. Mazur, Modeling the free solution electrophoretic mobility of short DNA fragments, Biopolymers 46 (1998) 359–373.
[19] S. Mazur, C. Chen, S.A. Allison, Modeling the electrophoresis of short duplex DNA: counterions K^+ and $Tris^+$, J. Phys. Chem. B 105 (2001) 1100–1108.
[20] S.A. Allison, C. Chen, D. Stigter, The length dependence of translational diffusion, free solution electrophoretic mobility, and electrophoretic tether force of rigid rod-like model duplex DNA, Biophys. J. 81 (2001) 2558–2568.
[21] D. Stigter, Mobility of water near charge interfaces, Adv. Colloid Interface Sci. 16 (1982) 253–265.
[22] D.C. Henry, The cataphoresis of suspended particles. Part I. The equation of cataphoresis, Proc. R. Soc. Lond. A. 203 (1931) 106–129.
[23] S.A. Allison, D. Stigter, A commentary on the screened-Oseen, counterion condensation formalism of polyion electrophoresis, Biophys. Chem. 78 (2000) 121–124.
[24] T.M. Ridgeway, D.B. Hayes, T.J. Wilson, et al., An apparatus for membrane-confined analytical electrophoresis, Electrophoresis 19 (1998) 1611–1619.
[25] T.M. Laue, H.K. Shepard, T.M. Ridgeway, T.P. Moody, T.J. Wilson, Membrane-confined analytical electrophoresis, in: G.K. Ackers, M.L. Johnson (Eds.), Methods in Enzymology, vol. 295, Academic Press, New York, 1998, pp. 494–518.
[26] S. Dao-Pin, E. Söderlind, W.A. Baase, J.A. Wozniak, U. Sauer, B.W. Matthews, Cumulative site-directed charge–charge replacements in bacteriophage T4 lysozyme suggest that long-range electrostatic interactions contribute little to protein stability, J. Mol. Biol. 221 (1991) 873–887.
[27] J.B. Matthews, F.R.N. Gurd, B. Garcia-Monreno, M.A. Flanagan, K.L. March, S.J. Shire, pH-dependent processes in proteins, CRC Crit. Rev. Biochem. 18 (2) (1985) 91–197.
[28] D.E. Anderson, The Role of Electrostatic Interactions in Stabilizing T4 Lysozyme, PhD Dissertation, University of Oregon, Eugene, OR, 1992.
[29] T.E. Creighton, Proteins (Structures and Molecular Properties), W.H. Freeman and Company, New York, 1983.
[30] I.H. Segel, Biochemical Calculations, 2nd ed., J. Wiley and Sons, New York, 1976.
[31] D.E. Anderson, W.J. Becktel, F.W. Dahlquist, pH denaturation of proteins: a single salt bridge contributes 3–5 kcal/mol to the free energy of folding of T4 lysozyme, Biochemistry 29 (1990) 2403–2408.
[32] N.C. Stellwagen, S. Magnusdottir, C. Gelfi, P.G. Righetti, Preferential counterion binding to A-tract DNA oligomers, J. Mol. Biol. 305 (2001) 1025–1033.
[33] S. Magnusdottir, H. Isambert, C. Heller, J. Viovy, Eletrodynamically induced aggregation during constant and pulsed field capillary electrophoresis of DNA, Biopolymers 49 (1999) 385–401.
[34] A. Tsugita, M. Inouye, Purification of bacteriophage T4 lysozyme, J. Biol. Chem. 243 (1968) 391–397.
[35] P. Schuck, B. Demeler, Direct sedimentation analysis of interference optical data in analytical ultracentrifugation, Biophysics 272 (1999) 199–208.
[36] T.M. Laue, Sedimentation equilibrium as a thermodynamic tool, in: G.K. Ackers, M.L. Johnson (Eds.), Methods in Enzymology, vol. 259, Academic Press, New York, 1995, pp. 427–452.
[37] T.M. Laue, T.M. Ridgeway, J.O. Wooll, et al., Insights from a new analytical electrophoresis apparatus, J. Pharm. Sci. 85 (1996) 1331–1335.
[38] J.E. Godfrey, Steady-state electrophoresis: a technique for measuring physical properties of macro-ions, Proc. Natl. Acad. Sci. USA 86 (1989) 4479–4483.
[39] T.M. Laue, A.L. Hazard, T.M. Ridgeway, D.A. Yphantis, Direct determination of macromolecular charge by equilibrium electrophoresis, Anal. Biochem. 182 (1989) 377–382.
[40] M.L. Johnson, J.J. Correia, D.A. Yphantis, H.R. Halvorson, Analysis of data from the analytical ultracentrifuge by nonlinear least-squares techniques, Biophys. J. 36 (1981) 575–588.
[41] T.M. Ridgeway, D.B. Hayes, A.L. Anderson, et al., Possible clinical applications for direct molecular charge determination by equilibrium electrophoresis, SPIE Proc. 2136 (1994) 263–274.
[42] H.X. Zhou, Macromolecular electrostatic energy within the non-linear Poisson–Boltzmann equation, J. Chem. Phys. 100 (1994) 3152–3162.
[43] B.J. Yoon, S. Kim, Electrophoresis of spheroidal particles, J. Colloid Interface Sci. 128 (1989) 275–288.
[44] B.J. Yoon, Electrophoretic motion of spherical particles with a non-uniform charge distribution, J. Colloid Interface Sci. 142 (1991) 575–581.
[45] S.A. Allison, V. Tran, Modeling the electrophoresis of rigid polyions: an application to lysozyme, Biophys. J. 68 (1995) 2261–2270.
[46] S.B. Smith, A.J. Bendich, Electrophoretic charge density and persistence length of DNA as measured by fluorescence microscopy, Biopolymers 29 (1990) 1167–1173.
[47] D. Stigter, C. Bustamante, Theory for the hydrodynamic and electrophoretic stretch of tethered B-DNA, Biophys. J. 75 (1998) 1197–1210.
[48] J.M. Garcia Bernal, J. Garcia de la Torre, Transport properties and hydrodynamic center of rigid macromolecules with arbitrary shapes, Biopolymers 19 (1980) 751–766.
[49] S.A. Allison, Boundary element modeling of biomolecular transport, Biophys. Chem. 93 (2001) 197–213.
[50] C. Tanford, Physical Chemistry of Macromolecules, Wiley, New York, 1971.
[51] E. Breslow, F.R.N. Gurd, Reactivity of sperm whale metmyoglobin towards hydrogen ions and *p*-nitrophenyl acetate, J. Biol. Chem. 237 (1962) 371–381.

[52] D.R. Linde (Ed.), CRC Handbook of Chemistry and Physics, 74th ed., CRC Press, Boca Raton, FL, 1993.
[53] J.A. Schellman, D. Stigter, Electrical double layer, zeta potential, and electrophoretic charge of double-stranded DNA, Biopolymers 16 (1977) 1415–1434.
[54] D. Stigter, A novel interpretation of steady-state electrophoresis experiments, J. Phys. Chem. B. 104 (2000) 3402–3403.
[55] M. Bier, Electrophoresis: Theory, Methods and Application, vol. II, Academic Press, New York, 1967, Chapter 1.
[56] H.B. Bull, An Introduction to Physical Biochemistry, F.A. Davis Company, Philadelphia, 1964, Chapter 13.
[57] L.B. Barnett, H.B. Bull, Electrophoresis of ribonuclease and of beta-lactoglobulin: isoelectric points of proteins, Arch. Biochem. Biophys. 89 (1960) 167–172.